


**Generalization of exceptional point conditions in perturbed coupled resonators**Shahab Ramezanpour <sup>1,\*</sup>, Andrey Bogdanov,<sup>1</sup> Andrea Alù,<sup>2,3</sup> and Younes Ra'di<sup>2</sup><sup>1</sup>*School of Physics and Engineering, ITMO University, St. Petersburg 197101, Russia*<sup>2</sup>*Advanced Science Research Center, City University of New York, 85 St. Nicholas Terrace, New York, New York 10031, USA*<sup>3</sup>*Physics Program, Graduate Center, City University of New York, New York, New York 10016, USA*

(Received 6 September 2021; revised 21 October 2021; accepted 25 October 2021; published 3 November 2021)

The phase singularity in open systems, known as the exceptional point (EP), has revealed exotic functionalities, especially in optics—as an illustration, ultrasensitive sensors and laser beam unidirectionality. The strong sensitivity to perturbations around the EP has been suggested for sensing applications. Nevertheless, the characteristics of such highly sensitive systems can be affected by unwanted perturbations during the fabrication process. However, if one can control perturbation, it can be considered as an additional degree of freedom to create and tune EPs, enabling fascinating phenomena. In this paper, we propose an analytical method to investigate such systems. We analytically derive the general conditions of EPs in the perturbed pair of coupled ring resonators, where both resonators can be perturbed by different scatterers. Several numerical examples are employed to verify the proposed analytical method. We propose a simple experimental scheme where the predicted effects can be confirmed. It is also shown that by changing the relative position of the scatterers with respect to each other, quite interesting states such as a chiral EP in one resonator or simultaneous chiral EPs in both resonators could be observed, making such a system a highly functional tunable device which can have several applications such as quantized reflection/transmission and  $q$ -bits.

DOI: [10.1103/PhysRevB.104.205405](https://doi.org/10.1103/PhysRevB.104.205405)**I. INTRODUCTION**

Unlike Hermitian systems, in which eigenvectors are orthogonal at degenerate eigenvalues, in non-Hermitian systems the eigenvectors are also degenerate (i.e., eigenvalues and eigenvectors coalesce simultaneously). This singularity in non-Hermitian systems is called the exceptional point (EP), leading to abrupt phase changes in the eigenvalue spectra. Such abrupt phase transitions around the EP in photonic systems lead to exotic functionalities such as laser mode selectivity and sensitivity enhancement [1–4].  $PT$ -symmetric systems can have entirely real eigenvalues, despite that they are non-Hermitian. However, beyond a critical condition, their eigenvalues become complex (broken  $PT$  symmetry), where this critical point has properties of the EP. In addition to lasing and sensing applications, parity-time symmetric systems enable robust wireless power transfer [5–7] and perfect absorption [8,9].

Exceptional point degeneracy can be realized in different optical and photonic systems supporting  $PT$ -symmetric schemes, such as a ridge optical waveguide where the loss is controlled by a Cr layer in half of it [10], and by a pair of coupled microtoroidal whispering-gallery-mode (WGM) resonators, where the gain in one of the resonators is achieved by  $\text{Er}^{3+}$  doping [11]. Instead of using (real) gain or loss, Ref. [12] proposes time modulation of an applied source as an equivalent to the gain or loss. This virtual  $PT$ -symmetric system [13] can have applications in critical coupling in high- $Q$  resonators

[14] and pulling force for a passive resonant object of any shape and composition [15]. Another mechanism to tune the energy spectra of a resonator is manipulating its geometry. By engineering the height and radius of a cylinder with a high refractive index, a high- $Q$  supercavity mode can be achieved by realizing the regime of bound states in the continuum [16,17]. This structure has shown a considerable enhancement of second harmonic generation [18]. The supercavity mode as well as EP can also be realized in a deformed shape of a cylindrical resonator [19]. Furthermore, an EP is achieved in parallel circular dielectric cylinders [20], two-layer cylindrical waveguides [21], graphene incorporated multilayer metamaterials [22], nonlinear non-Hermitian systems [23–27], and arrays of particles [28,29].

Due to the high sensitivity of such systems, small perturbations during the fabrication process can considerably affect the aforementioned singularity, therefore resulting in a need for an additional element such as a heating scheme for fine-tuning of the resonators [3]. On the contrary, gaining control over the perturbations and being able to engineer them can open significant degrees of freedom in engineering the desired responses, such as chiral EPs and high- $Q$  multifunctional resonators. It was recently shown that by employing two nanoparticles (which can be considered as a perturbation) along the surface of a microresonator, and tuning their positions, the backscattering from CW (CCW) to CCW (CW) can be removed (CW: clockwise; CCW: counterclockwise), and as a result, the resonator will support only CW (CCW) modes at this specific condition, which can be associated with the appearance of so-called chiral states [30–32]. This asymmetric backscattering and nonorthogonal modes can also be achieved

\*shahab.ramezanpour@metalab.ifmo.ru

in a resonator incorporating notches [33], or in a deformed resonator [34,35]. Furthermore, it was shown that employing scatterers or notches in coupled resonators can give rise to new functionalities such as EP-assisted absorption/transparency [36], and enhancement of laser emission directionality [37].

In this paper, perturbations are considered as an additional degree of freedom to create degeneracy in these systems, which may be lifted due to fabrication imperfections. Also, they can be utilized to create fascinating phenomena which can have application in unidirectional lasing, high- $Q$  resonators, and sensors. We derive general conditions that can bring a perturbed pair of coupled resonators to the EP regime. With engineering the perturbations, we can generate EPs in the system, and these expressions can be useful to study the effect of unwanted perturbations which may arise during the fabrication process. Regarding the perturbation values, the location of the EP can be tuned in parameter space, and the amount of loss/gain can be varied. Besides, with engineering the position of the scatterers, some interesting field distributions such as a chiral EP in one resonator, individually, and both of them simultaneously are observed in the structure, making the system a tunable device which can shift from one state to another one by changing the position of the scatterers. Furthermore, to confirm the method, the numerical result from COMSOL is compared to coupled mode theory (CMT).

## II. A COUPLED PAIR OF RESONATORS: ONE PERTURBED AND ONE UNPERTURBED

We work with a system of coupled resonators supporting WGMs. To generalize the result, we use dimensionless parameters, then suggest a possible physical system. Perturbation along the surface of a disk or ring can give rise to both clockwise (CW) and counterclockwise (CCW) modes with different field amplitudes. In a pair of resonators, the CW (CCW) mode in the first disk excites a CCW (CW) mode in the second one, as shown schematically in Fig. 1(a). Therefore, utilizing coupled mode theory [38,39], such system can be described using the following equations:

$$\frac{da_1}{dt} = (-i\omega_1 - \gamma_1)a_1 - i\kappa_{12}a_2 - i\kappa_{ab}b_2, \quad (1a)$$

$$\frac{da_2}{dt} = (-i\omega_1 - \gamma_1)a_2 - i\kappa_{21}a_1 - i\kappa_{ab}b_1, \quad (1b)$$

$$\frac{db_1}{dt} = (-i\omega_2 - \gamma_2)b_1 - i\kappa_{ab}a_2, \quad (1c)$$

$$\frac{db_2}{dt} = (-i\omega_2 - \gamma_2)b_2 - i\kappa_{ab}a_1. \quad (1d)$$

In this set of equations  $\kappa_{ab}$  is the coupling rate between two rings. In the first ring,  $\kappa_{12}$  and  $\kappa_{21}$  are the coupling rates from CCW to CW and CW to CCW modes, respectively, which exist due to the presence of the scatterer beside the resonator (even without the scatterers, we can observe a coupling between CW and CCW in each resonator due to the coupling between the resonators, which can usually be ignored). We note that there is no coupling (or negligible coupling) between CW and CCW in the second ring, since in this system the second ring is unperturbed. If we assume a monochromatic excitation, we can consider  $d/dt \rightarrow -i\mu$ ; therefore, Eq. (1)

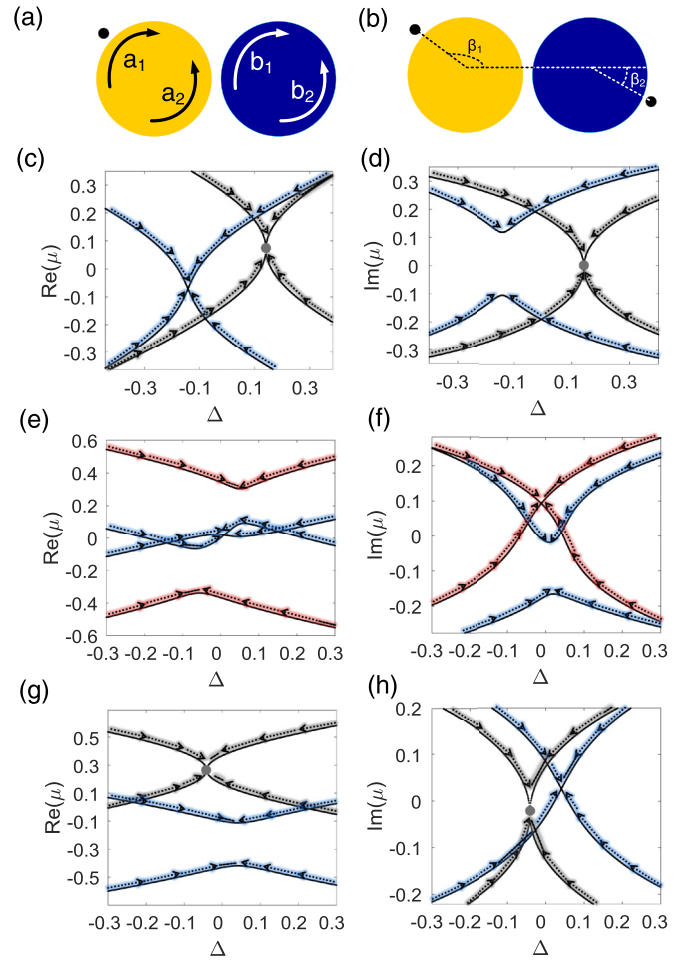


FIG. 1. Evolution of the eigenvalues, with gray (blue and red) curves leading (not leading) to EP degeneracy. Panels (c)–(d) and (e)–(h) belong to Secs. II and III, respectively. (a) Perturbation in the first resonator. (b) Perturbation in both resonators. Perturbation in one ring: (c) Real and (d) imaginary part of eigenvalue for  $\kappa_{ab} = 0.5, \kappa_{12} = 0.1 - 0.01i, \kappa_{21} = 0.2 - 0.015i, \delta = 2\kappa_{ab} - \text{Im}(\sqrt{\kappa_{12}\kappa_{21}})$ . Perturbation in both rings: (e) Real and (f) imaginary part of eigenvalue for  $\kappa_{ab} = 0.5, \kappa_{12} = 0.2 - 0.01i, \kappa_{21} = 0.3 - 0.02i, \kappa'_{12} = 0.35 - 0.05i, \kappa'_{21} = 0.1 - 0.01i$ , and  $\delta$  is considered from Eq. (9b). (g) Real and (h) imaginary parts of eigenvalue for  $\kappa'_{12} = 0.35 - 0.05i, \kappa'_{21} = 0.2336 - 0.0294i$ , while the other parameters are the same as before. EP occurs at  $\Delta = -0.041$  which corresponds to Eq. (9a).

can be written as an eigenvalue problem, where the complex frequency of the resonators is considered  $\Omega_1 = \omega_1 - i\gamma_1$  and  $\Omega_2 = \omega_2 - i\gamma_2$ :

$$\mu \begin{pmatrix} a_1 \\ a_2 \\ b_1 \\ b_2 \end{pmatrix} = \begin{pmatrix} \Omega_1 & \kappa_{12} & 0 & \kappa_{ab} \\ \kappa_{21} & \Omega_1 & \kappa_{ab} & 0 \\ 0 & \kappa_{ab} & \Omega_2 & 0 \\ \kappa_{ab} & 0 & 0 & \Omega_2 \end{pmatrix} \begin{pmatrix} a_1 \\ a_2 \\ b_1 \\ b_2 \end{pmatrix}. \quad (2)$$

The eigenvalues of the system can be calculated using

$$\begin{vmatrix} \Omega_1 - \mu & \kappa_{12} & 0 & \kappa_{ab} \\ \kappa_{21} & \Omega_1 - \mu & \kappa_{ab} & 0 \\ 0 & \kappa_{ab} & \Omega_2 - \mu & 0 \\ \kappa_{ab} & 0 & 0 & \Omega_2 - \mu \end{vmatrix} = 0. \quad (3)$$

After some mathematical manipulation, we can get the following characteristic equations:

$$(\Omega_1 - \mu)(\Omega_2 - \mu) - \kappa_{ab}^2 = \sqrt{\kappa_{12}\kappa_{21}}(\Omega_2 - \mu), \quad (4a)$$

$$(\Omega_1 - \mu)(\Omega_2 - \mu) - \kappa_{ab}^2 = -\sqrt{\kappa_{12}\kappa_{21}}(\Omega_2 - \mu). \quad (4b)$$

Using Eq. (4a), we can derive the two eigenvalues of the system as

$$2\mu = \Omega_1 + \Omega_2 - \kappa \pm \sqrt{(\Omega_1 + \Omega_2 - \kappa)^2 - 4(\Omega_1\Omega_2 - \kappa\Omega_2 - \kappa_{ab}^2)}, \quad (5)$$

where  $\kappa = \sqrt{\kappa_{12}\kappa_{21}}$  is defined. To have an EP, these eigenvalues should be degenerate, which can happen if  $(\Omega_1 + \Omega_2 - \kappa)^2 - 4(\Omega_1\Omega_2 - \kappa\Omega_2 - \kappa_{ab}^2) = 0$ . This condition can be written as a quadratic polynomial of  $\Omega_2 - \Omega_1$ :  $(\Omega_2 - \Omega_1)^2 + 2\kappa(\Omega_2 - \Omega_1) + \kappa^2 + 4\kappa_{ab}^2 = 0$ , from which we can derive a condition connecting corresponding complex frequencies and couplings  $\Omega_2 - \Omega_1 = -\kappa \pm 2i\kappa_{ab}$ . Applying the same procedure to Eq. (4b), we get a second condition on complex frequencies as  $\Omega_2 - \Omega_1 = \kappa \pm 2i\kappa_{ab}$ . Rephrasing these two conditions, we can derive the general conditions of the EP:

$$\Delta = \omega_2 - \omega_1 = \text{Re}(\sqrt{\kappa_{12}\kappa_{21}}), \quad (6a)$$

$$\delta = \gamma_2 - \gamma_1 = \pm 2\kappa_{ab} - \text{Im}(\sqrt{\kappa_{12}\kappa_{21}}), \quad (6b)$$

or

$$\Delta = \omega_2 - \omega_1 = -\text{Re}(\sqrt{\kappa_{12}\kappa_{21}}), \quad (7a)$$

$$\delta = \gamma_2 - \gamma_1 = \pm 2\kappa_{ab} + \text{Im}(\sqrt{\kappa_{12}\kappa_{21}}). \quad (7b)$$

This reveals that for real values of  $\kappa$ , the EP can happen at two locations  $\Delta = \omega_2 - \omega_1 = -\kappa$  and  $\Delta = \omega_2 - \omega_1 = \kappa$  for  $\delta = \gamma_2 - \gamma_1 = \pm 2\kappa_{ab}$ .

As an illustrative example, Figs. 1(c) and 1(d) show the real and imaginary parts of the eigenvalues as a function of  $\Delta$  [plotted using Eqs. (4)], for  $\kappa_{12} = 0.1 - 0.01i$ ,  $\kappa_{21} = 0.2 - 0.015i$ ,  $\kappa_{ab} = 0.5$ , and  $\delta = 2\kappa_{ab} - \text{Im}(\sqrt{\kappa_{12}\kappa_{21}})$  (we consider  $\omega_1 = \omega_0 - \Delta/2$  and  $\omega_2 = \omega_0 + \Delta/2$ , where  $\omega_0$  can be an arbitrary value). This shows that the exceptional point occurs at  $\Delta = \text{Re}(\sqrt{\kappa_{12}\kappa_{21}}) = 0.1414$ , which corresponds to the analytical results in Eqs. (6a)–(6b) (note that the EPs are shown by gray dots).

In the analytical model, we have considered no coupling between CW (CCW) from one resonator and CW (CCW) from another resonator,  $\kappa_{cw,12} = \kappa_{cw,21} = 0$  ( $\kappa_{ccw,12} = \kappa_{ccw,21} = 0$ ). Our numerical calculations confirm the accuracy of this assumption. For specific configurations, such as a scatterer in the coupling region between two resonators, the amount of these couplings can be nonzero (but still small). Our analysis shows that we can still obtain an EP for nonzero and specific values of these couplings. However, in such a scenario the complexity of the problem increases, and deriving closed-form analytical conditions for the EP would be more challenging.

### III. A COUPLED PAIR OF RESONATORS: BOTH PERTURBED

In the previous section, we considered a system of a coupled pair of resonators where one of the resonators was perturbed due to the presence of a scatterer next to it, while the other resonator was unperturbed. Here, we consider a more complex scenario where both resonators are perturbed through different scatterers [see Fig. 1(b)]. This system can be described using the following equation:

$$\mu \begin{pmatrix} a_1 \\ a_2 \\ b_1 \\ b_2 \end{pmatrix} = \begin{pmatrix} \Omega_1 & \kappa_{12} & 0 & \kappa_{ab} \\ \kappa_{21} & \Omega_1 & \kappa_{ab} & 0 \\ 0 & \kappa_{ab} & \Omega_2 & \kappa'_{12} \\ \kappa_{ab} & 0 & \kappa'_{21} & \Omega_2 \end{pmatrix} \begin{pmatrix} a_1 \\ a_2 \\ b_1 \\ b_2 \end{pmatrix}, \quad (8)$$

where, compared to Eq. (2), an additional coefficient  $\kappa'_{12}$  ( $\kappa'_{21}$ ) is employed to take into account the coupling between CCW (CW) and CW (CCW) in the second ring. Following the same procedure as in the previous section, we can derive the required conditions for EPs (detailed derivations are provided in the Appendix):

$$\Delta = \omega_2 - \omega_1 = \text{Re}(\sqrt{\kappa_{12}\kappa_{21}} - \sqrt{\kappa'_{12}\kappa'_{21}}), \quad (9a)$$

$$\delta = \gamma_2 - \gamma_1 = \pm 2\kappa_{ab} - \text{Im}(\sqrt{\kappa_{12}\kappa_{21}} - \sqrt{\kappa'_{12}\kappa'_{21}}), \quad (9b)$$

$$\kappa_{12}/\kappa_{21} = \kappa'_{21}/\kappa'_{12}. \quad (9c)$$

Another set of equations is

$$\Delta = \omega_2 - \omega_1 = -\text{Re}(\sqrt{\kappa_{12}\kappa_{21}} - \sqrt{\kappa'_{12}\kappa'_{21}}), \quad (10a)$$

$$\delta = \gamma_2 - \gamma_1 = \pm 2\kappa_{ab} + \text{Im}(\sqrt{\kappa_{12}\kappa_{21}} - \sqrt{\kappa'_{12}\kappa'_{21}}), \quad (10b)$$

$$\kappa_{12}/\kappa_{21} = \kappa'_{21}/\kappa'_{12}. \quad (10c)$$

As can be seen from these conditions, in comparison to the EP conditions for the scenario considered in the previous section, here we have additional conditions relating the couplings between CW and CCW in different resonators [Eqs. (9c) and (10c)]. As an illustrative example, Figs. 1(e) and 1(f) show real and imaginary parts of eigenvalues for  $\kappa_{ab} = 0.5$ ,  $\kappa_{12} = 0.2 - 0.01i$ ,  $\kappa_{21} = 0.3 - 0.02i$ ,  $\kappa'_{12} = 0.35 - 0.05i$ ,  $\kappa'_{21} = 0.1 - 0.01i$ , and  $\delta$  is calculated from Eq. (9b). Note that, here, we intentionally consider a case where the last condition of the EP in Eqs. (9) and (10) is not satisfied (i.e.,  $\kappa_{12}/\kappa_{21} \neq \kappa'_{21}/\kappa'_{12}$ ). The results in Figs. 1(e) and 1(f) show that the real (imaginary) parts coalesce while the imaginary (real) parts depart, which is shown by blue (red) arrows, proving that the EP cannot be achieved if the last condition is not satisfied.

Now let us consider the case where all the conditions for the EP are satisfied, including the last condition (i.e.,  $\kappa_{12}/\kappa_{21} = \kappa'_{21}/\kappa'_{12}$ ). Figures 1(g) and 1(h) show the eigenvalue for  $\kappa'_{12} = 0.35 - 0.05i$ ,  $\kappa'_{21} = 0.2336 - 0.0294i$  ( $\kappa_{12}/\kappa_{21} = \kappa'_{21}/\kappa'_{12}$ ) (other parameters are the same as before), where the EP occurs at  $\Delta = -0.041$ , which corresponds to Eq. (9a).

## IV. PRACTICAL SCHEME

### A. One scatterer

Here, we study the EP condition in a coupled pair of resonators which contain one scatterer. In what follows, we use full-wave numerical simulations using COMSOL Multiphysics to analyze the eigenvalue problem in this structure. First, we obtained the numerical value of the unperturbed resonance frequency  $\Omega_0 = 859.42$  THz for an isolated single resonator (the unit of eigenvalues; therefore, the components of the Hamiltonian are in THz, although they could be converted to rad/sec as well as being unitless). Next, we analyzed the isolated single resonator with one scatterer in its vicinity, and obtained two eigenmodes of this structure with eigenvalues  $\mu_1 = 858.88 + 0.40i$  THz and  $\mu_2 = 859.20$  THz. Now we can calculate the coupling between CW and CCW modes that happens due to the presence of the scatterer next to the resonator. The Hamiltonian of this structure corresponds to  $H = \begin{pmatrix} \Omega_1 & \kappa_{12} \\ \kappa_{21} & \Omega_1 \end{pmatrix}$ , where  $\Omega_1 = \Omega_0 + V_1 + U_1$ ,  $\kappa_{12} = (V_1 - U_1)e^{-i2m\beta_1}$ , and  $\kappa_{21} = (V_1 - U_1)e^{i2m\beta_1}$ . In these expressions,  $\Omega_0$  is the resonant frequency of the unperturbed resonator, while  $\beta_1$  and  $m$  represent the azimuthal position of the scatterer and azimuthal wave number of the WGM in the resonator, respectively [31]. The eigenvalues of this Hamiltonian are  $\mu_{1,2} = \Omega_1 \pm \sqrt{\kappa_{12}\kappa_{21}}$ . By substituting the expressions for  $\kappa_{12}$ ,  $\kappa_{21}$ , and  $\Omega_1$ , the eigenvalues can be rewritten as  $\mu_1 = \Omega_0 + 2V_1$  and  $\mu_2 = \Omega_0 + 2U_1$ . We note that the real part of both  $V_1$  and  $U_1$  is negative since by utilization of the scatterer, the effective radius of the resonator would be increased, and its effective resonant frequencies would be reduced. On the other hand, in derivation of the Hamiltonian, initially the scatterer is assumed to be in the zero degree ( $\beta_1 = 0$ ), and the perturbation variables  $V_1$  and  $U_1$  are inserted in the Hamiltonian as frequency shift of even and odd modes, respectively. Thus, the rotation of the scatterer would be considered as an exponential function of  $\beta_1$ . Since the scatterer at zero degrees affects the even mode more than the odd mode, the absolute value of the real part of  $V_1$  is larger than  $U_1$ , leading to  $\sqrt{\kappa_{12}\kappa_{21}} = |V_1 - U_1| = U_1 - V_1$ . By substituting the values for  $\Omega_0 = 859.42$  THz,  $\mu_1 = 858.88 + 0.40i$  THz, and  $\mu_2 = 859.20$  THz obtained from the numerical simulations, we can calculate  $V_1 = -0.27 + 0.20i$  THz and  $U_1 = -0.11$  THz.

To calculate the coupling rate between two resonators, we analyzed a pair of coupled similar and unperturbed resonators, which yields two eigenmodes with eigenvalues  $\mu_1 = 859.89$  THz,  $\mu_2 = 858.99$  THz (note that there are two other modes as well, with degenerated eigenvalues). The associated Hamiltonian can be written as  $H = \begin{pmatrix} \Omega_0 & \kappa \\ \kappa & \Omega_0 \end{pmatrix}$  with eigenvalues  $\mu_1 = \Omega_0 - \kappa$ ,  $\mu_2 = \Omega_0 + \kappa$ . We already know the resonance frequency of a single resonator ( $\Omega_0 = 859.42$  THz) and eigenfrequencies of the coupled pair of unperturbed resonators ( $\mu_{1,2} = 859.05$  THz,  $859.81$  THz) from the numerical simulations. By substituting these values, we find the coupling rate  $\kappa \approx 0.38$  THz. The coupling coefficients can also be calculated based on the physical system under consideration, e.g., using a lumped wire model in a coupled rod geometry [40].

In our numerical example, by adjusting the refractive index and radius of the second resonator, we tune the structure to work at the EP [Fig. 2(a) shows the field distribution of this

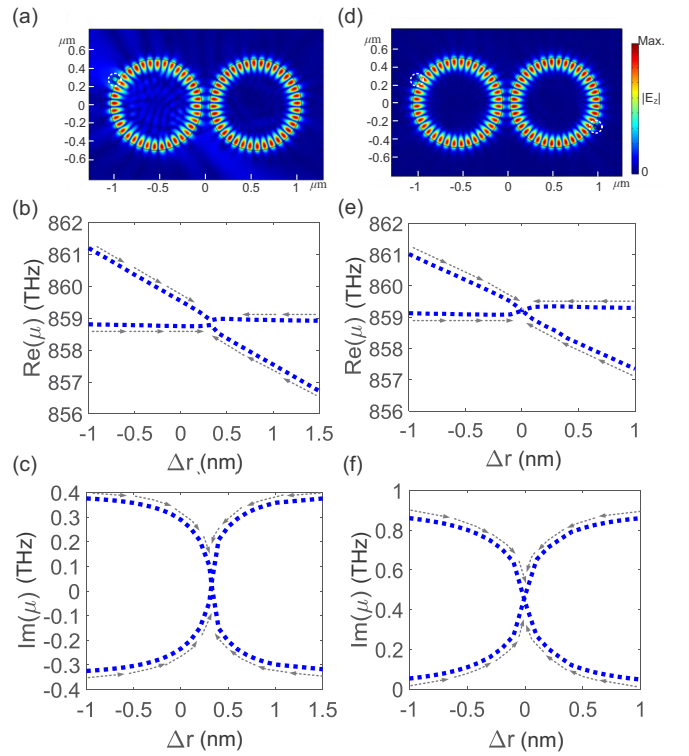


FIG. 2. (a) Eigenmode of coupled resonator with one scatterer in EP. (b) Real and (c) imaginary parts of eigenvalue of coupled resonators with one scatterer. (d) Eigenmode of coupled resonator with two scatterers in EP. (e) Real and (f) imaginary parts of eigenvalue of coupled resonators with two scatterers.

structure in the EP]. Figures 2(b)–2(c) show the real and imaginary parts of the eigenvalues of the coupled resonator with one scatterer vs  $\Delta r = r_2 - r_1$ , where the radius and refractive index of the first resonator are set to  $r_1 = 0.5 \mu\text{m}$  and  $n_1 = 2.45$ , and the refractive index of the second resonator is tuned to  $n_2 = 2.45 - 0.001i$ . The gap between the resonators and position of the scatterer are set to  $g = 0.86 \mu\text{m}$  and  $\varphi = 148^\circ$ . These results show that the closest value to the EP occurs at around  $\Delta r = 0.33$  nm. Therefore, the tuned radius and refractive index for the second resonator for the whole structure to operate at EP are  $r_2 = 500.33$  nm and  $n_2 = 2.45 - 0.001i$ , respectively. We then remove the scatterer and the first resonator to find the complex resonance frequency of the second resonator ( $\Omega_2$ ). The corresponding complex resonance frequency for the second resonator is  $\Omega_2 = 858.85 - 0.35i$  THz.

### 1. Comparison between numerical and analytical results

Now that we have numerically derived all the complex frequencies and coupling coefficients for the simulated example at the EP, we can verify the analytical EP conditions that we presented in the previous sections. As was shown in Sec. II, in order to have an EP in the coupled resonators with one scatterer along the surface of the left resonator, Eqs. (6a)–(6b) or (7a)–(7b) should be fulfilled. According to Eq. (7a), the difference of the real parts of the resonant frequencies should be equal to  $\omega_2 - \omega_1 = -\text{Re}(\sqrt{\kappa_{12}\kappa_{21}}) = \text{Re}(V_1) - U_1$ . Since

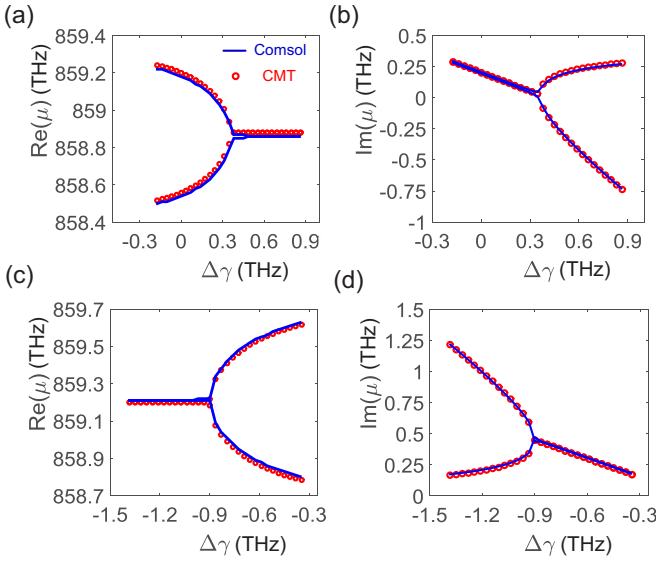


FIG. 3. Comparison of COMSOL and CMT results for the structure with one scatterer: (a) Real and (b) imaginary, and two scatterers: (c) real and (d) imaginary parts of eigenvalues.

$\omega_1 = \Omega_0 + \text{Re}(V_1) + U_1$ , we can obtain

$$\omega_2 = \Omega_0 + 2 \text{Re}(V_1) = 858.88 \text{ THz}. \quad (11)$$

Similarly, according to Eq. (7b), the difference of imaginary parts of resonant frequencies should be  $\gamma_2 - \gamma_1 = 2\kappa + \text{Im}\sqrt{\kappa_{12}\kappa_{21}} = 2\kappa - \text{Im}(V_1)$ . Since  $\gamma_1 = -\text{Im}(V_1)$ , we get

$$\gamma_2 = 2\kappa - 2 \text{Im}(V_1) = 0.36 \text{ THz}. \quad (12)$$

The resonant frequency and dissipation of the second resonator in Eqs. (11) and (12) are very close to the value obtained from the COMSOL result  $\Omega_2 = 858.85 - 0.35i$  THz, at the EP, which verifies the calculated EP conditions in Sec. II.

Figures 3(a) and 3(b) represent a more complete comparison between the COMSOL results with those obtained from the coupled mode theory presented in Sec. II. For this comparison, instead of radius, we tune the imaginary part of the refractive index of the second resonator, since by changing the radius, some other parameters such as resonance frequency, loss, and coupling between two resonators can change simultaneously. Also, it should be noted that in this figure, the eigenvalues are plotted versus the difference of the (intrinsic) dissipation of the resonators  $\Delta\gamma = \gamma_2 - \gamma_1$  with  $\gamma_1 = 0$ .

For the structure with one scatterer, the setting of the simulation is the same as in Figs. 2(b)–2(c), but with fixed radius  $r_2 = 500.33$  nm (at which the EP can occur). The imaginary part of the second resonator's refractive index is tuned (for which the corresponding complex frequency is obtained by analyzing a single resonator with such refractive indices). For CMT, we consider the eigenvalue problem, Eq. (2), with  $\Omega_1 = \Omega_0 + V_1 + U_1$ ,  $\kappa_{12} = (V_1 - U_1)e^{-i2m\beta_1}$ ,  $\kappa_{21} = (V_1 - U_1)e^{i2m\beta_1}$ ,  $\Omega_2 = \Omega_0 + 2\text{Re}(V_1) - i\gamma_2$ . The even- and odd-mode frequency shifts are  $V_1 = -0.27 + 0.20i$  THz and  $U_1 = -0.11$  THz, respectively, angular momentum of the resonators is  $m = 18$ , azimuthal rotation of the scatterer is  $\beta_1 = 148^\circ$ , resonant frequency  $\Omega_0 = 859.42$  THz, and

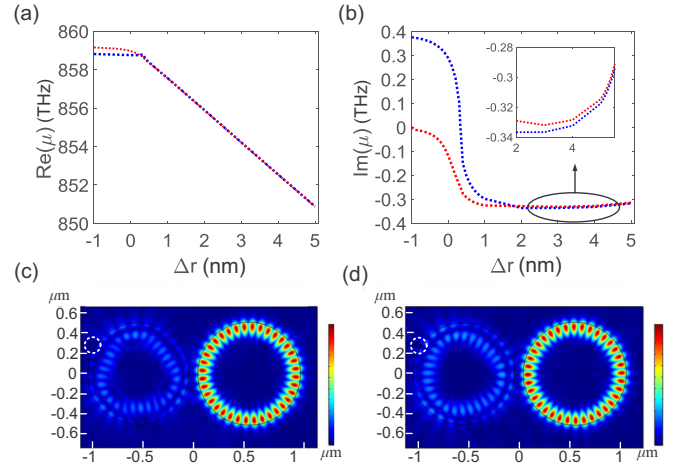


FIG. 4. (a)–(b) Real and imaginary parts of eigenvalues of symmetric and antisymmetric modes. (c)–(d) Field distribution of the chiral EP.

coupling between two resonators with distance  $g = 0.86 \mu\text{m}$  is estimated  $\kappa = 0.38$  THz. Figure 3 shows good agreement between COMSOL and CMT results for the structure with one scatterer.

## 2. Chiral exceptional point

The chiral EP is an interesting type of EP that has been shown to occur, e.g., in an individual resonator incorporating two scatterers along its surface [31]. Such EP is due to the destructive optical interferences for either CW or CCW modes. A similar effect can be observed in a coupled pair of resonators with one scatterer. The perturbed coupled resonators have four eigenmodes: two symmetric and two antisymmetric. If the eigenvalues of one symmetric and one antisymmetric mode degenerate [see Figs. 4(a) and 4(b), right resonator], we will observe the chiral EP in this structure. The associated field distribution is shown in Figs. 4(c)–4(d) for  $\Delta r = 5.5$  nm. Besides, the field distribution in the left resonator is seemingly a linear combination of two WGMs with different radial and azimuthal quantum numbers, with a specific weighting coefficient. We note that in this figure, just below  $\Delta r = 2$  nm, there is a coincidence point. However, at this point the eigenfunctions of two modes are orthogonal (even- and odd-mode resonances); therefore, it cannot be considered an EP, for which both eigenvalues and eigenfunctions should coalesce.

## B. Two scatterers

In this section, we investigate the EP in a pair of coupled resonators containing two scatterers (one next to each scatterer). We consider the simplest form when two scatterers as well as the radius of the resonators are identical. Knowing  $\kappa_{12} = (V_1 - U_1)e^{-i2m\beta_1}$ ,  $\kappa_{21} = (V_1 - U_1)e^{i2m\beta_1}$ ,  $\kappa'_{12} = (V_1 - U_1)e^{-i2m\beta_2}$ ,  $\kappa'_{21} = (V_1 - U_1)e^{i2m\beta_2}$ , the term  $\sqrt{\kappa_{12}\kappa_{21}} - \sqrt{\kappa'_{12}\kappa'_{21}}$  in Eqs. (9) and (10) would be zero. Therefore, the condition of Eq. (9c) or (10c) yields  $2m(\beta_1 + \beta_2) = n\pi$  where  $n$  is an integer number, which can happen for specific rotations of the scatterers. For instance, the rotation of the first and second scatterers is considered  $150^\circ$  and  $-30^\circ$ , respectively, while the angular momentum is  $m = 18$ , which

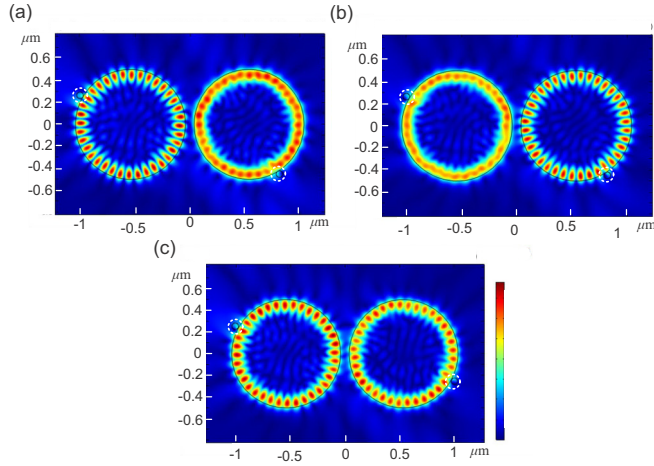


FIG. 5. Chiral EP in (a) the right resonator, (b) left resonator, and (c) both resonators.

fulfills the aforementioned condition. Figure 2(d) shows the field distribution of this structure in the EP, and Figs. 2(e) and 2(f) show real and imaginary parts of its eigenvalues versus  $\Delta r = r_2 - r_1$ , where the EP happens at  $\Delta r = 0$ . The radius of the first resonator and gap between them are  $r_1 = 0.5 \mu\text{m}$  and  $g = 0.8 \mu\text{m}$ , while their refractive indices are tuned to  $n_1 = 2.45$  and  $n_2 = 2.45 + 0.0026i$ , respectively.

Figures 3(c) and 3(d) verify that the presented CMT in Sec. III perfectly describes the coupled pair of resonators with two scatterers. For two scatterers, the settings of the simulation in COMSOL are the same as in Figs. 2(e)–2(f), but with fixed radius  $r_2 = 0.5 \mu\text{m}$ , and different values of the imaginary part of the second resonator's refractive index. For CMT, Eq. (8) is used with  $\Omega_1 = \Omega_0 + V_1 + U_1$ ,  $\kappa_{12} = (V_1 - U_1)e^{-i2m\beta_1}$ ,  $\kappa_{21} = (V_1 - U_1)e^{i2m\beta_1}$ ,  $\Omega_2 = \Omega_0 + V_1 + U_1 - i\gamma_2$ ,  $\kappa'_{12} = (V_1 - U_1)e^{-i2m\beta_2}$ ,  $\kappa'_{21} = (V_1 - U_1)e^{i2m\beta_2}$ . The azimuthal rotation of the first and second scatterers is  $\beta_1 = 150^\circ$  and  $\beta_2 = -30^\circ$ , and the coupling rate of two resonators with distance  $g = 0.8 \mu\text{m}$  is  $\kappa = 0.43 \text{ THz}$ .

The chiral EP can also occur in the coupled resonators with two scatterers. It is quite interesting to note that by tuning the relative position of the scatterers, we can achieve a chiral EP in one of the resonators, individually, or both of them, simultaneously. Switching between these two states can be done by changing the position of the scatterers.

Figure 5 shows different states of the chiral EP in this structure, which are obtained by tuning the position of the scatterers. The refractive indices of the left and right resonators are considered  $n_1 = 2.45$  and  $n_2 = 2.45 + 0.0023i$ , respectively. In Figs. 5(a), 5(b), and 5(c), the chiral EP occurs in the right resonator, left resonator, and both of them, where the azimuthal position of the scatterers ( $\varphi_1, \varphi_2$ ) is tuned to  $(150^\circ, -58.5^\circ)$ ,  $(150^\circ, -58^\circ)$ , and  $(148.5^\circ, -28.5^\circ)$ , respectively. In Fig. 5(c), the gap between the scatterers and the resonators ( $g_1, g_2$ ) is tuned to (2,3) nm, while in Figs. 5(a) and 5(b), there is no gap.

## V. CONCLUSION AND OUTLOOK

We found three general EP conditions in the perturbed coupled pair of resonators, and showed that, with manipulating

the perturbation, we can achieve the EP regime, if the system fulfills these conditions. Our analytical model reveals several exciting phenomena about the operational mechanism of these structures. It shows that the location of the EP can be tuned by the value of the perturbation, and we can achieve the EP in a system with any arbitrary value of perturbations as far as the mentioned conditions are satisfied. We studied a few numerical examples using full-wave numerical simulations to validate the presented analytical method. The numerical results show that the presented analytical method can describe the system with a very high accuracy. Having control over the perturbation can enable engineering fascinating functionalities such as creating a chiral EP in only one resonator as well as both of them, simultaneously.

The more sophisticated Hamiltonian contains the effect of the scatterer in the vicinity of one resonator on the other resonator, which will be the subject of future works. For instance, numerical results show that some specific positions of the scatterer yield closer conditions to the EP, compared to the other positions, which can only be described by the indirect effect of the scatterers on the intercoupling between the resonators, and on the coupling between CW (CCW) and CCW (CW) of another resonator. To deal with such Hamiltonian, with a considerable number of variables, some methods such as deep learning can be incorporated, which was recently employed in the photonics community to design various sophisticated structures. Besides, the scatterers in the coupling region between the resonators can create some other interesting results, such as chiral modes of higher-order resonances.

## ACKNOWLEDGMENTS

This work has been partially supported by the Air Force Office of Scientific Research MURI program and the Simons Foundation. The work is supported by the Russian Science Foundation (21-12-00383). A.B. acknowledges the BASIS Foundation.

## APPENDIX

Setting the determinant of matrix Eq. (8) to zero gives

$$\begin{aligned} & [(\Omega_1 - \mu)(\Omega_2 - \mu) - \kappa_{ab}^2]^2 \\ & = +\kappa'_{12}\kappa'_{21}(\Omega_1 - \mu)^2 + \kappa_{12}\kappa_{21}(\Omega_2 - \mu)^2 \\ & \quad - \kappa_{12}\kappa_{21}\kappa'_{12}\kappa'_{21} + \kappa_{ab}^2\kappa_{12}\kappa'_{12} + \kappa_{ab}^2\kappa_{21}\kappa'_{21}. \end{aligned} \quad (\text{A1})$$

If we assume  $\kappa_{12}\kappa'_{12} = \kappa_{21}\kappa'_{21}$  [in fact, this assumption gives one of the conditions of the EP, Eq. (9c) or (10c)], we can write

$$\begin{aligned} & [(\Omega_1 - \mu)(\Omega_2 - \mu) - \kappa_{ab}^2]^2 \\ & = [\sqrt{\kappa'_{12}\kappa'_{21}}(\Omega_1 - \mu) + \sqrt{\kappa_{12}\kappa_{21}}(\Omega_2 - \mu)]^2 \\ & \quad - 2\kappa_{12}\kappa'_{12}(\Omega_1 - \mu)(\Omega_2 - \mu) - (\kappa_{12}\kappa'_{12})^2 \\ & \quad + 2\kappa_{ab}^2\kappa_{12}\kappa'_{12}, \end{aligned} \quad (\text{A2})$$

which gives

$$\begin{aligned} & [(\Omega_1 - \mu)(\Omega_2 - \mu) - \kappa_{ab}^2 + \kappa_{12}\kappa'_{12}]^2 \\ & = [\sqrt{\kappa'_{12}\kappa'_{21}}(\Omega_1 - \mu) + \sqrt{\kappa_{12}\kappa_{21}}(\Omega_2 - \mu)]^2. \end{aligned} \quad (\text{A3})$$

This equation can be decoupled to two second-order polynomial equations. Following the same procedure as in Sec. II, one of these equations gives  $\Omega_2 - \Omega_1 =$

$\sqrt{\kappa_{12}\kappa_{21}} - \sqrt{\kappa'_{12}\kappa'_{21}} \pm 2i\kappa_{ab}$ , and another one gives  $\Omega_2 - \Omega_1 = \sqrt{\kappa'_{12}\kappa'_{21}} - \sqrt{\kappa_{12}\kappa_{21}} \pm 2i\kappa_{ab}$  for EP conditions, which is equivalent to Eqs. (9a)–(9b) and (10a)–(10b), respectively.

- 
- [1] C. M. Bender and S. Boettcher, Real Spectra in Non-Hermitian Hamiltonians having  $PT$  Symmetry, *Phys. Rev. Lett.* **80**, 5243 (1998).
- [2] M.-A. Miri and A. Alù, Exceptional points in optics and photonics, *Science* **363**, eaar7709 (2019).
- [3] H. Hodaei, A. U. Hassan, S. Wittek, H. Garcia-Gracia, R. El-Ganainy, D. N. Christodoulides, and M. Khajavikhan, Enhanced sensitivity at higher-order exceptional points, *Nature (London)* **548**, 187 (2017).
- [4] Z. Xiao, H. Li, T. Kottos, and A. Alù, Enhanced Sensing and Nondegraded Thermal Noise Performance Based on  $PT$ -Symmetric Electronic Circuits with a Sixth-Order Exceptional Point, *Phys. Rev. Lett.* **123**, 213901 (2019).
- [5] S. Assaworrorarit, X. Yu, and S. Fan, Robust wireless power transfer using a nonlinear parity-time-symmetric circuit, *Nature (London)* **546**, 387 (2017).
- [6] Y. Ra'di, B. Chowkwale, C. Valagiannopoulos, F. Liu, A. Alù, C. R. Simovski, and S. A. Tretyakov, On-site wireless power generation, *IEEE Trans. Antennas Propag.* **66**, 4260 (2018).
- [7] Z. Xiao, Y. Ra'di, S. Tretyakov, and A. Alù, Microwave tunneling and robust information transfer based on parity-time-symmetric absorber-emitter pairs, *Research* **2019**, 7108494 (2019).
- [8] C. Wang, W. R. Sweeney, A. D. Stone, and L. Yang, Coherent perfect absorption at an exceptional point, *Science* **373**, 1261 (2021).
- [9] S. Xiao, J. Gear, S. Rotter, and J. Li, Effective  $PT$ -symmetric metasurfaces for subwavelength amplified sensing, *New J. Phys.* **18**, 085004 (2016).
- [10] A. Guo, G. J. Salamo, D. Duchesne, R. Morandotti, M. Volatier-Ravat, V. Aimez, G. A. Siviloglou, and D. N. Christodoulides, Observation of  $PT$ -Symmetry Breaking in Complex Optical Potentials, *Phys. Rev. Lett.* **103**, 093902 (2009).
- [11] B. Peng, S. K. Özdemir, F. Lei, F. Monifi, M. Gianfreda, G. L. Long, S. Fan, F. Nori, C. M. Bender, and L. Yang, Parity-time-symmetric whispering-gallery microcavities, *Nat. Phys.* **10**, 394 (2014).
- [12] H. Li, H. Moussa, D. Sounas, and A. Alù, Parity-Time Symmetry Based on Time Modulation, *Phys. Rev. Appl.* **14**, 031002 (2020).
- [13] H. Li, A. Mekawy, A. Krasnok, and A. Alù, Virtual Parity-Time Symmetry, *Phys. Rev. Lett.* **124**, 193901 (2020).
- [14] Y. Ra'di, A. Krasnok, and A. Alù, Virtual critical coupling, *ACS Photonics* **7**, 1468 (2020).
- [15] S. Lepeshov and A. Krasnok, Virtual optical pulling force, *Optica* **7**, 1024 (2020).
- [16] M. V. Rybin, K. L. Koshelev, Z. F. Sadrieva, K. B. Samusev, A. A. Bogdanov, M. F. Limonov, and Y. S. Kivshar, High- $Q$  Supercavity Modes in Subwavelength Dielectric Resonators, *Phys. Rev. Lett.* **119**, 243901 (2017).
- [17] M. Odit, K. Koshelev, S. Gladyshev, K. Ladutenko, Y. Kivshar, and A. Bogdanov, Observation of supercavity modes in subwavelength dielectric resonators, *Adv. Mater.* **33**, 2003804 (2021).
- [18] K. Koshelev, S. Kruk, E. M.-Gaykazyan, J.-H. Choi, A. Bogdanov, H.-G. Park, and Y. Kivshar, Subwavelength dielectric resonators for nonlinear nanophotonics, *Science* **367**, 288 (2020).
- [19] W. Yan, P. Lalanne, and M. Qiu, Shape Deformation of Nanoresonator: A Quasinormal-Mode Perturbation Theory, *Phys. Rev. Lett.* **125**, 013901 (2020).
- [20] A. Abdrabou and Y. Lu, Exceptional points for resonant states on parallel circular dielectric cylinders, *J. Opt. Soc. Am. B* **36**, 1659 (2019).
- [21] Y. Huang, Y. Shen, and G. Veronis, Non- $PT$ -symmetric two-layer cylindrical waveguide for exceptional-point-enhanced optical devices, *Opt. Express* **27**, 37494 (2019).
- [22] Q. Liu, B. Wang, S. Ke, H. Long, K. Wang, and P. Lu, Exceptional points in Fano-resonant graphene metamaterials, *Opt. Express* **25**, 7203 (2017).
- [23] D. Witthaut, E. M. Graefe, S. Wimberger, and H. J. Korsch, Bose-Einstein condensates in accelerated double-periodic optical lattices: Coupling and crossing of resonances, *Phys. Rev. A* **75**, 013617 (2007).
- [24] G. Wunner, H. Cartarius, P. Koeberle, J. Main, and S. Rau, Exceptional points for nonlinear Schrödinger equations describing Bose-Einstein condensates of ultracold atomic gases, *Acta Polytechnica* **51**, 95 (2011).
- [25] P. Djourwe, Y. Pennec, and B. Djafari-Rouhani, Frequency locking and controllable chaos through exceptional points in optomechanics, *Phys. Rev. E* **98**, 032201 (2018).
- [26] H. Ramezani and T. Kottos, Unidirectional nonlinear  $PT$ -symmetric optical structures, *Phys. Rev. A* **82**, 043803 (2010).
- [27] S. Ramezanpour and A. Bogdanov, Tuning exceptional points with Kerr nonlinearity, *Phys. Rev. A* **103**, 043510 (2021).
- [28] J.-H. Park, J.-H. Park, A. Ndao, W. Cai, L. Hsu, A. Kodigala, T. Lepetit, Y.-H. Lo, and B. Kanté, Symmetry-breaking-induced plasmonic exceptional points and nanoscale sensing, *Nat. Phys.* **16**, 462 (2020).
- [29] M. Y. Nada, M. A. K. Othman, and F. Capolino, Theory of coupled resonator optical waveguides exhibiting high-order exceptional points of degeneracy, *Phys. Rev. B* **96**, 184304 (2017).
- [30] J. Zhu, S. K. Özdemir, L. He, and L. Yang, Controlled manipulation of mode splitting in an optical microcavity by two Rayleigh scatterers, *Opt. Express* **18**, 23535 (2010).
- [31] J. Wiersig, Structure of whispering-gallery modes in optical microdisks perturbed by nanoparticles, *Phys. Rev. A* **84**, 063828 (2011).
- [32] B. Peng, S. K. Özdemir, M. Liertzer, W. Chen, J. Kramer, H. Yilmaz, J. Wiersig, S. Rotter, and L. Yang, Chiral modes and directional lasing at exceptional points, *Proc. Natl. Acad. Sci. USA* **113**, 6845 (2016).
- [33] J. Wiersig, S. W. Kim, and M. Hentschel, Asymmetric scattering and nonorthogonal mode patterns in optical microspirals, *Phys. Rev. A* **78**, 053809 (2008).
- [34] J. Kullig and J. Wiersig, High-order exceptional points of counterpropagating waves in weakly deformed microdisk cavities, *Phys. Rev. A* **100**, 043837 (2019).

- [35] J. Wiersig, A. Eberspächer, J.-B. Shim, J.-W. Ryu, S. Shinohara, M. Hentschel, and H. Schomerus, Nonorthogonal pairs of co-propagating optical modes in deformed microdisk cavities, *Phys. Rev. A* **84**, 023845 (2011).
- [36] C. Wang, X. Jiang, G. Zhao, M. Zhang, C. W. Hsu, B. Peng, A. D. Stone, L. Jiang, and L. Yang, Electromagnetically induced transparency at a chiral exceptional point, *Nat. Phys.* **16**, 334 (2020).
- [37] Q. Zeng, E. Lafalce, C. H. Lin, M. J. Smith, J. Jung, Y. Yoon, Z. Lin, V. V. Tsukruk, and Z. V. Vardeny, Control of whispering gallery modes and  $PT$ -symmetry breaking in colloidal quantum dot microdisk lasers with engineered notches, *Nano Lett.* **19**, 6049 (2019).
- [38] H. Haus and W. Huang, Coupled-mode theory, *Proc. IEEE* **79**, 1505 (1991).
- [39] B. E. Little, S. T. Chu, H. A. Haus, J. Foresi, and J.-P. Laine, Microring resonator channel dropping filters, *J. Lightwave Technol.* **15**, 998 (1997).
- [40] A. C. Tasolamprou, O. Tsilipakos, M. Kafesaki, C. M. Soukoulis, and E. N. Economou, Toroidal eigenmodes in all-dielectric metamolecules, *Phys. Rev. B* **94**, 205433 (2016).